Chemistry & Biology, Vol. 10, 1267–1279, December, 2003, ©2003 Elsevier Science Ltd. All rights reserved. DOI 10.1016/j.chembiol.2003.11.014

Small Molecule Modulation of the Human Chromatid Decatenation Checkpoint

Stephen J. Haggarty,[1,2,3] Kathryn M. Koeller,[2,3] Tweeny R. Kau,[5] Pamela A. Silver,[5] Michel Roberge,[6] and Stuart L. Schreiber[1,2,3,4,*]

[1]Departments of Molecular and Cellular Biology
[2]Departments of Chemistry and Chemical Biology
[3]ICB-Initiative for Chemical Genetics
[4]Howard Hughes Medical Institute
Harvard University
12 Oxford Street
Cambridge, Massachusetts 02138
[5]Department of Biological Chemistry and Molecular Pharmacology
Harvard Medical School and
Department of Cancer Biology
The Dana Farber Cancer Institute
Boston, Massachusetts 02115
[6]Department of Biochemistry and Molecular Biology
University of British Columbia
Vancouver, British Columbia V6T 1Z3
Canada

Summary

After chromosome replication, the intertwined sister chromatids are disentangled by topoisomerases. The integrity of this process is monitored by the chromatid decatenation checkpoint. Here, we describe small molecule modulators of the human chromatid decatenation checkpoint identified using a cell-based, chemical genetic modifier screen. Similar to 1,2,7-trimethylyxanthine (caffeine), these small molecules suppress the G(2)-phase arrest caused by ICRF-193, a small molecule inhibitor of the enzymatic activity of topoisomerase II. Analysis of specific suppressors, here named suptopins for *sup*pressor of *Top*oisomerase II *in*hibition, revealed distinct effects on cell cycle progression, microtubule stability, nucleocytoplasmic transport of cyclin B1, and no effect on the chromatin deacetylation checkpoint induced by trichostatin A. The suptopins provide new molecular tools for dissecting the role of topoisomerases in maintaining genomic stability and determining whether inhibiting the chromatid decatenation checkpoint sensitizes tumor cells to chemotherapeutics.

Introduction

The maintenance of genomic stability in eukaryotic cells involves an evolutionarily conserved set of signaling networks termed cell cycle checkpoints [1, 2]. These networks function to detect incompletely replicated, damaged, or abnormally structured deoxyribonucleic acid (DNA) and to arrest cell cycle progression to allow for repair or cell death. Elucidating the molecular basis for the activation and fidelity of these checkpoints is important for understanding genomic stability and for the development of improved strategies for the treatment of diseases involving aberrant cell proliferation or alterations of chromosomal DNA.

An important component to the maintenance of genomic stability is the proper separation of newly replicated sister chromatids prior to chromosome segregation during mitosis (M phase) [3–5]. Sister chromatids are composed of DNA complexed with histones and a variety of associated proteins that collectively constitute chromatin. During DNA replication (S phase), sister chromatids become highly concatenated (intertwined) along their lengths because the replicating strands of DNA exist in a coil (Figure 1A) [2, 6]. In order to form individualized chromosomes in preparation for chromosome segregation, sister chromatids are decatenated starting in the G_2 phase of the cell cycle by the activity of evolutionarily conserved proteins known as type II topoisomerases (TopoII) [6–9]. This process involves the formation of a double-strand DNA break and covalent linkage of the 5′ phosphoryl group of each DNA strand to form a protein-tyrosyl intermediate (Figure 1A). These transformations are followed by the passing of a second intact DNA strand through the break and the rejoining of the double-stranded break (Figure 1A).

In addition to their importance as basic research tools, small molecules targeting the TopoII family are important clinically as cancer chemotherapeutics and as antimicrobial agents [7, 9, 10]. One class of small molecules targeting TopoII, which includes doxorubicin and ellipticine (Figure 1B), interfere with its DNA rejoining activity by stabilizing a covalent TopoII-DNA complex. Treatment of mammalian cells with this class of small molecules results in widespread DNA damage due to double-stranded breaks and the activation of the DNA damage-induced G_1 and/or G_2 checkpoints [1, 2, 11–14]. Another class of small molecules targeting TopoII, which includes ICRF-193 (meso-2,3-bis[2,6-dioxopiperazin-4-yl]butane) (Figure 1C), inhibits its enzymatic activity, thereby trapping TopoII in a "closed-clamp" rather than in a TopoII-DNA covalent complex [10, 15]. This conformational state of TopoII occurs after strand passage and DNA religation but before the hydrolysis of adenosine triphosphate, which prevents the additional decatenation necessary for entry into mitosis. As a result, cells arrest in the G_2 phase due to the activation of what has been referred to as the chromatid decatenation checkpoint [16–21].

Unlike the DNA damage-induced or mitotic spindle assembly checkpoints, there appears to be no counterpart to the chromatid decatenation checkpoint in the budding or fission yeast [2]. Consequently, understanding the molecular mechanisms of this checkpoint has lagged behind that of other checkpoints. From the original discovery by Downes et al. [16], the signal transduction leading to cell cycle arrest in response to ICRF-193 was found to be sensitive to the small molecule 1,2,7-trimethylyxanthine (caffeine) and to the structural analog

*Correspondence: stuart_schreiber@harvard.edu

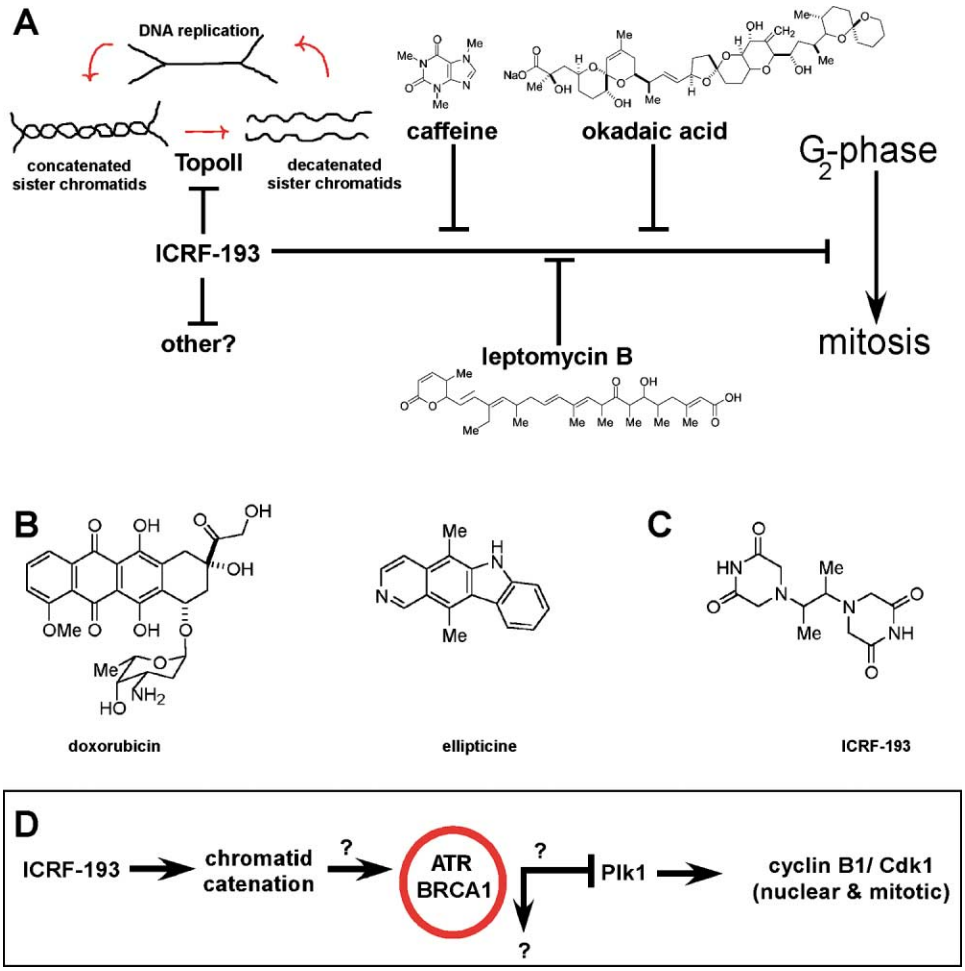

Figure 1. Overview of the Chromatid Decatenation Checkpoint and the Topoisomerase II-Dependent Regulation of Entry into Mitosis

(A) Schematic of the role of TopoII in catalyzing the decatenation of sister chromatids and structures of small molecules known to suppress the DNA damage-independent (caffeine [16, 22, 24], leptomycin [18]) and DNA damage-dependent (okadaic acid [23]) G_2 checkpoint activated upon treatment with TopoII inhibitors.

(B) Chemical structures of two inhibitors of TopoII that stabilize covalent TopoII-DNA complexes.

(C) Chemical structure of ICRF-193 (meso-2,3-bis[2,6-dioxopiperazin-4-yl]butane), an inhibitor of the enzymatic activity of TopoII, which traps it in a closed-clamp conformation.

(D) Components of the network regulating the ICRF-193-induced chromatid decatenation checkpoint (modified from [18] and [20]).

2-aminopurine [22]. Addition of caffeine to ICRF-193-treated cells produces aberrant mitotic figures with abnormally elongated and intertwined chromatids containing a core scaffold of chromosomal proteins [18, 22]. Evidence for the importance of phosphorylation in the chromatid decatenation checkpoint was demonstrated by the ability of the protein phosphatase 1 and 2A inhibitors (e.g., okadaic acid, Figure 1A) to overcome the G_2 arrest [23]. More recently, the signal generated by ICRF-193 treatment was shown to be independent of the phosphatidylinositol 3′ kinase family member ATM (ataxia telangiectasia mutated) and p53 [18, 21] but dependent upon ATR (ATM and radiation arrest deficient 3-related) signaling, which is known to be inhibited by caffeine (Figure 1D) [24–26]. In turn, ATR activation, through a mechanism involving the tumor suppressor BRCA1, was proposed to inhibit polo-like kinase 1 (Plk1) activity, resulting in altered nucleocytoplasmic transport of cyclin B1 [20]. Consistent with this finding, leptomycin B (an inhibitor of nuclear export [27]) or overexpression of cyclin B1 [18] bypassed the ICRF-193-induced arrest, presumably through affecting the equilibrium of active nuclear and cytoplasmic complexes of cyclin B1/Cdk1 involved in regulating mitotic entry [28].

Besides detecting insufficient decatenation of sister chromatids, a DNA damage-independent G_2 checkpoint delays the entry of cells into mitosis in response to aberrant acetylation of chromatin [30, 31]. This chromatin deacetylation checkpoint is induced upon treatment of cells with histone deacetylase (HDAC) inhibitors, such as trichostatin A [31–33]. This checkpoint appears to be absent in a number of tumor cell lines, which may be relevant to the differential sensitivity of different tumor cell lines [31] to treatment with HDAC inhibitors. In the case of trichostatin A, the cell cycle arrest can be suppressed by a set of 23 recently described small mole-

cules [33]. The targets of these small molecules may include components of the signaling network required for cell cycle arrest. Complexes containing TopoII possess HDAC and chromatin remodeling activities [34, 35]. However, the relationship between the decatenation checkpoint and the chromatin deacetylation checkpoint remains poorly understood.

To discover small molecule modulators of the human chromatid decatenation checkpoint and to clarify its relationship to the chromatin deacetylation checkpoint, we took an approach similar to that used to identify small molecule modulators of the DNA-damage-induced G_2 checkpoint [36–39] and trichostatin A-induced cell cycle arrest [33]. This approach relies on the logic of classical genetics in which the identification of suppressor and enhancers of a particular phenotype has been a fruitful means to identify systematically components of complex biochemical networks.

Results

A chemical genetic modifier screen was performed using a cytoblot assay (described in full in [40]) to identify small molecules that modify the cellular effects of ICRF-193 (Figure 1C), resulting in suppression (bypass) of the decatenation checkpoint and entry into mitosis. As a model mammalian cell type, A549 lung carcinoma cells were used because they are adherent and possess an intact chromatid decatenation checkpoint that can be activated by ICRF-193. After screening 9600 small molecules ($\sim$20 μM) and two rounds of retesting, a total of 20 small molecules reproducibly increased the number of A549 cells capable of entering mitosis in the presence of ICRF-193 (Figure 2).

To investigate the relationship between different cell cycle checkpoints, the data from this chromatid decatenation checkpoint screen were compared with those from the chromatin deacetylation checkpoint (trichostatin [TSA]-modifier) [33] and mitotic screens [41, 42]. This comparison involved the same 9600 small molecules used at the same concentration and in the same cells. In total, 132 compounds were active in at least one of the three assays (Figure 3A). Hierarchical clustering of the distance matrix, computed from using the Tanimoto coefficient, classified the small molecules into four sets (Figure 3B). Anti-mitotics (causing an arrest in the mitotic state) comprise the largest set, the majority of which cause microtubule destabilization, resulting in activation of the spindle assembly checkpoint [41]. Two small molecules scored in the anti-mitotic and TSA-modifier screen [33]. No small molecules, however, scored in the ICRF-193 assay and any other assay, or in all three assays.

Positions of ICRF-193 Suppressors on a Global Map of Chemical Space

To determine global similarities/differences between the regions of chemical space selected by the ICRF-193-modifier, TSA-modifier, and anti-mitotic screens, the 132 biologically active small molecules were coded according to the clustering of the screening data. A set of molecular descriptors was then computed for these and the other library members screened in at least one of the three assays. After removing descriptors with no variance, a total of 155 graph-theoretic, information-theoretic, or physiochemical descriptors were considered for each small molecule. Since many of these molecular descriptors are redundant, principal component analysis (PCA) was used to reduce the dimensionality of the descriptor space to a set of linearly independent, composite descriptors that best represent the variance of the data [43, 44]. The resulting representation provides a global, linear model of the information describing the structures of the small molecules. The components of the first three eigenvectors were used to position each of the small molecules in a reduced 3-D chemical space. Accordingly, this model accounted for a total of 37% of the variance in the molecular descriptors, with the full dimensionality spanning 147 dimensions instead of the original 155 (see Supplemental Figure S1 online at http://www.chembiol.com/cgi/content/full/10/12/1267/DC1/). Using the coding determined by the clustering of the biological assay data, one of four colors was assigned to each of the different classes of biologically active small molecules, yielding a mapping of biological measurement space onto chemical space (Figure 3C). Figure 3D depicts a composite distribution of the 132 biologically active small molecules (left) and inactive small molecules that segments the chemical space studied into "coding" (those molecules that cause a phenotype) and "noncoding" (those molecules that do not cause a phenotype or have not been tested) regions.

Diversity of ICRF-193 Suppressors

One approach to proceeding with the characterization of the ICRF-193 suppressors was to choose small molecules based upon their potency. However, our previous experience with identifying small molecules functioning through different mechanisms highlighted the shortcomings of simply selecting the most potent hits for further characterization. For example, the twelve most potent anti-mitotics selected from the screen of the same library as studied here all shared the same intracellular target (tubulin), with monastrol, an inhibitor of Eg5, being identified as a weak anti-mitotic in the primary screen [41, 42]. An alternative approach is to choose small molecules based upon different structural classes. Visual inspection of the 3-D chemical structures that are shown in Figure 2D reveals similarities between certain molecules; however, such an ad hoc approach is unable to compare quantitatively a large number of structures and properties. To make selections in an unbiased and more quantitative fashion, the assumption was made of an inverse relationship between the distance spanning two small molecules in a 3-D PCA model of the associated chemical space and the likelihood that the small molecules target the same component of the underlying signaling network. To determine quantitatively these relationships, the molecular descriptors used in the global model of the chemical space were compiled for the local region of chemical space containing only the suppressors of ICRF-193, and PCA was performed again. After removing descriptors with zero variance, a total of 159 descriptors were considered. The first three dimensions

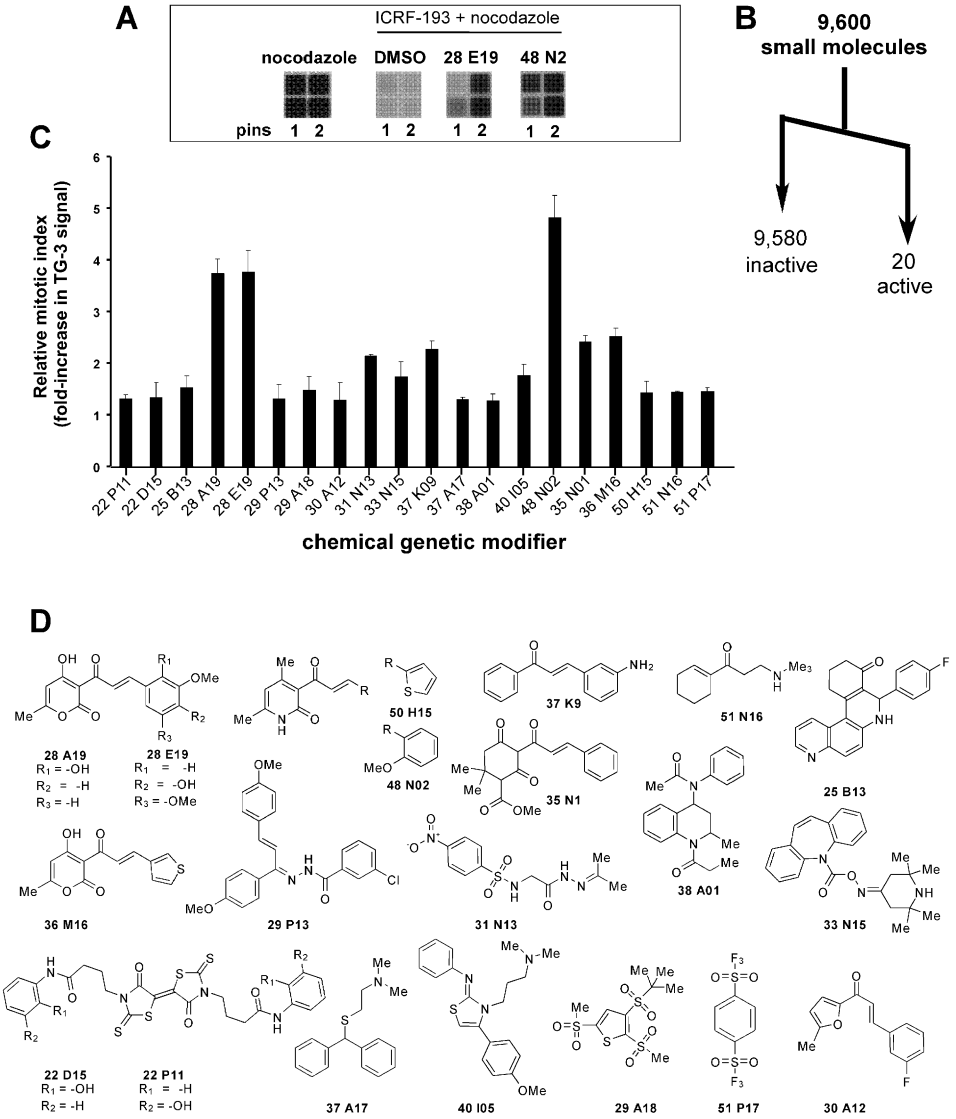

Figure 2. Summary of a Chemical Genetic Modifer Screen of 9600 Small Molecules for Suppressors of ICRF-193

(A) Film exposure of cytoblot assay using the TG-3 mAb. A549 cells have an intact chromatid decatenation checkpoint that can be activated by addition of ICRF-193 (7 μM) and suppressed by two of the modifiers of ICRF-193 (1 pin ~25-50 μM, two pins ~50 μM). Nocodazole (332 nM) was added at the time of addition of suppressors to trap cells that have bypassed the chromatid decatenation checkpoint and entered mitosis.

(B) Summary of screening results after two rounds of retesting using the TG-3 mAb cytoblot assay.

(C) Example of retest data for the 20 suppressors (two pin transfers; ~25–50 μM) showing the average (n = 2) value of TG-3 signal relative to the DMSO (n = 10) control alone (labels correspond to structures shown in (D). Error bars correspond to one standard deviation of the mean. Increased TG-3 signal corresponds to increased bypass of the decatenation checkpoint and accumulation in mitosis. Small molecules that had a TG-3 mAb signal equal to (or greater than) the mean plus 1.5 standard deviations of DMSO treated control cells (in at least two independent retests) were considered to be biologically active.

(D) Chemical structures of 20 small molecule suppressors of the ICRF-193-induced chromatid decatenation checkpoint. Small molecules characterized further in this work are: 22 P11 (suptopin-1), 28 E19 (suptopin-2), and 33 N15 (suptopin-3).

in the reduced space accounted for a total of 55% of the variance in the molecular descriptors, with the full dimensionality spanning 21 dimensions instead of the original 159 (Figure 4A). The set of ICRF-193 suppressors is therefore less diverse than the whole library. The coordinates of the compounds in the 21-D reduced space were then used to construct a Euclidean distance matrix, which was then subject to hierarchical clustering. From this analysis, three distinct clusters emerged within the graph (green arrows) (Figure 4C) from which the small molecules named suptopin-1, suptopin-2, and suptopin-3 (for *sup*pressor of *top*oisomerase *in*hibition) were selected for further cell biological analysis (Figure 4D).

Mitotic Spreads and Immunofluorescence

Although the screen we used had the capacity to identify small molecules directly targeting components of the

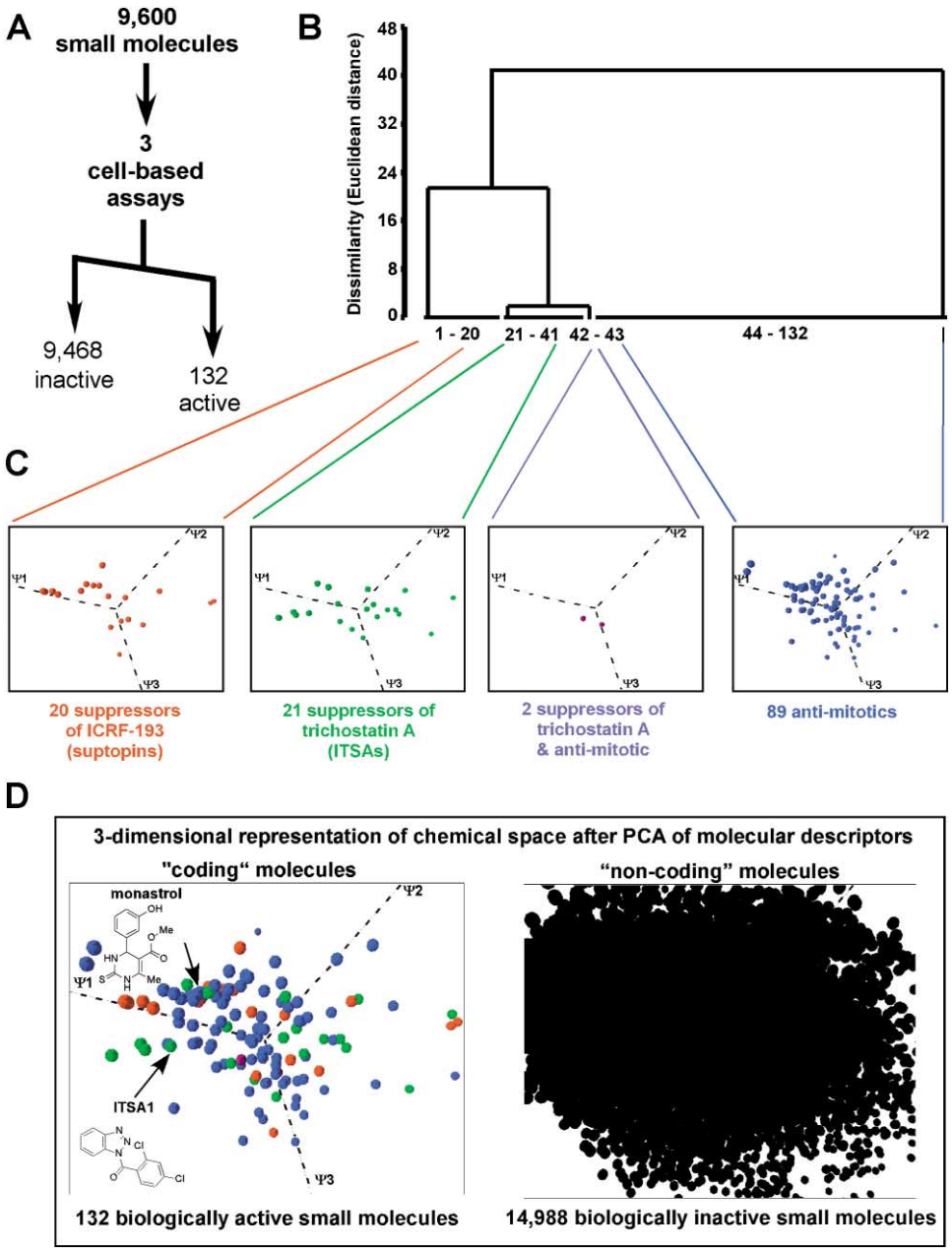

Figure 3. Multidimensional Analysis of Three Cell-Based Screens of 9600 Small Molecules: Suppressors of ICRF-193, Suppressors of Trichostatin A, and Anti-mitotics.

(A) Summary of combined screening results.

(B) Hierarchical clustering of biological assay data depicting four clusters of small molecules corresponding to 20 suppressors of ICRF-193, 21 suppressors of ITSA1, 89 anti-mitotics, and 2 small molecules that scored in both the anti-mitotic and trichostatin suppressor screen.

(C) Position of the four clusters of small molecules in a 3-D molecular descriptor space formed from the first three principal components (PCA) axes (Ψ1–Ψ3), which account for 37% of the total variation in the data. Axes shown run parallel to indicated PCA axes.

(D) Composite representations of chemical space depicting biologically active (coding) and inactive (noncoding) small molecules colored based upon the clustering of assay data from cell-based assays for suppressors of ICRF-193 (red), suppressors of trichostatin (green), and anti-mitotics (blue). Axes shown run parallel to indicated PCA axes (see Supplemental Figure S1 for an enlarged representation of the entire chemical space of the 15,120 small molecules).

chromatid decatenation checkpoint (e.g., as caffeine does with ATR), the assay itself is an indirect measure based upon the level of the phosphorylated epitope recognized by the TG-3 mAb [36]. Consequently, small molecules that scored positive in the primary assay might affect directly the phosphorylation status of proteins that are recognized by the TG-3 mAb. Furthermore, although no compounds scored in both ICRF-193-modifier and anti-mitotic screens (Figure 3B), additional phenotypic effects at higher concentrations/durations of

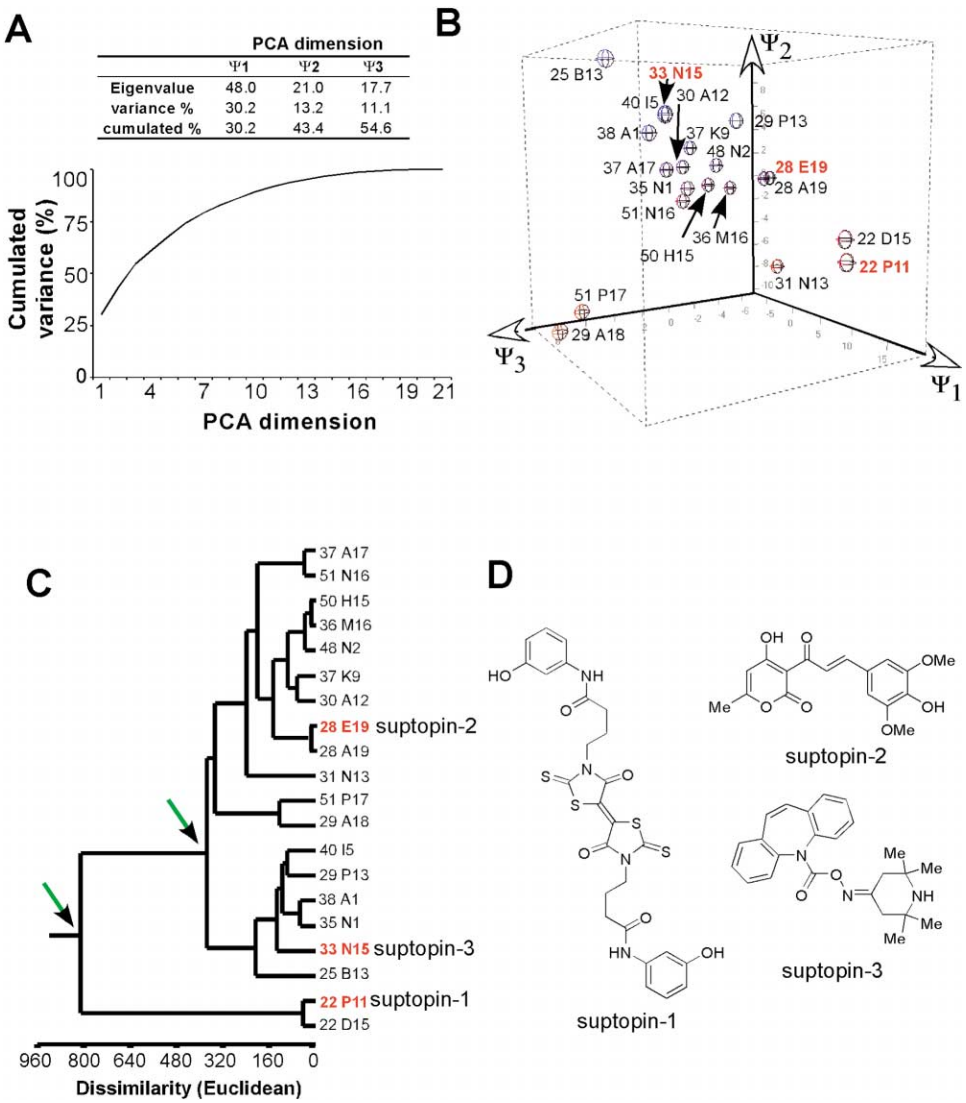

Figure 4. Principal Component Analysis of a 159-D Chemical Space Derived from the Molecular Descriptors of the ICRF-193 Suppressors

(A) Variance accounted for by each eigenvalue/eigenvector and plot of cumulated variance of the reduced 21-D space.

(B) Positions of the 20 ICRF-193 suppressors according to their coordinates from the first three PCA axes (Ψ1–Ψ3). Shading (blue to red) indicates increased weighting on Ψ1.

(C) Hierarchical clustering of the 20 ICRF-193 suppressors showing three main clusters (green arrows) of small molecules from which suptopin-1 to -3 were chosen for further analysis.

(D) Chemical structures of suptopin-1 to -3.

treatment or unexpected effects due to synergy with nocodazole might occur. To explore these possibilities, mitotic spreads were performed on cells treated with suptopin-1, -2, or -3 (Figures 5A and 5B). In the absence of ICRF-193, neither caffeine nor suptopin-3 had an effect on the percentage of mitotic cells compared to the control solvent dimethylsulphoxide (DMSO) alone. In contrast, both suptopin-1 and suptopin-2 caused an increase in the number of mitotic cells, with the resulting chromosomes hypercondensed compared to normal mitotic chromosomes. The fact that suptopin-1 and suptopin-2 caused a mitotic defect in the absence of ICRF-193 but did not score as anti-mitotics in the original assay is likely due to differences in concentration and duration of treatment. In the presence of ICRF-193, the number of mitotic cells was decreased compared to the DMSO control, as expected due to the dominance of ICRF-193 pretreatment over the anti-mitotic effect of nocodazole. Upon the addition of caffeine, suptopin-2, or suptopin-3, there was a strong increase in the number of mitotic cells compared to DMSO, whereas suptopin-1 had a weaker effect and caused some visible cell death. In contrast to the hypercondensed chromosomes seen upon treatment of cells with only suptopin-2, cells treated with suptopin-2 in the presence of ICRF-193 appeared to have elongated chromosomes with paired sister chromatids. This chromosomal morphology was similar to the effect of caffeine and suptopin-3.

To test for additional phenotypic effects, A549 cells treated with suptopin-1 to -3 were fixed and incubated

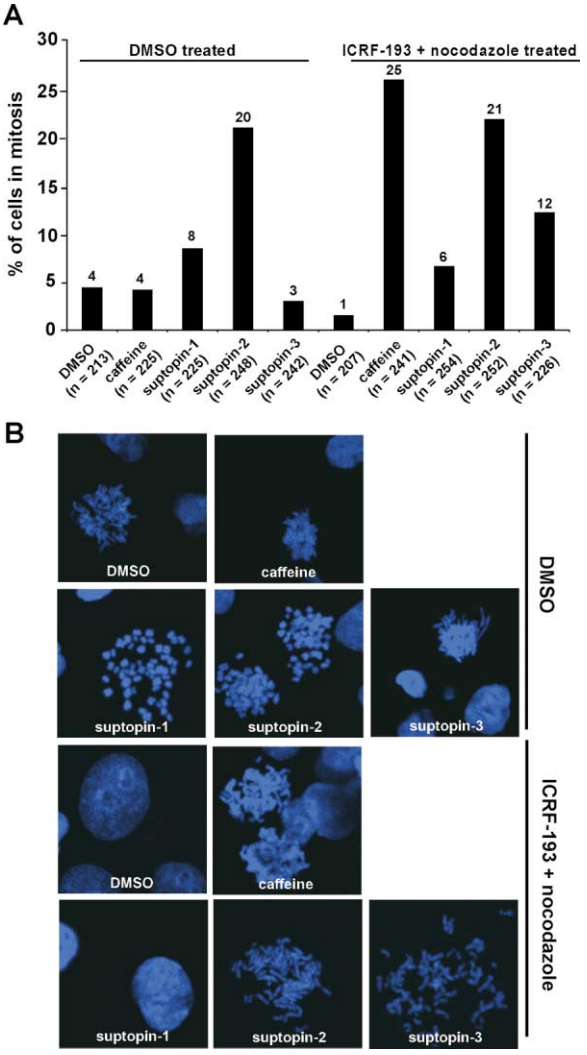

Figure 5. Effect of the Suptopins on the Mitotic Index and Chromosomal Morphology of A549 Cells

(A) Mitotic index obtained from counting the frequency of mitotic cells (n = total number of cells counted in two independent treatments). All cells received an equivalent concentration of DMSO. Nocodazole (332 nM) was added at the time of addition of the suppressors only to ICRF-193 (7 μM) pretreated (5 hr) cells, and cells were incubated an additional 18 hr. Suptopin-2 (60 μM, 20 μg/mL) and to a lesser extent suptopin-1 (32 μM, 20 μg/mL) increased the mitotic index both in the absence and presence of ICRF-193. Caffeine (2 mM) and suptopin-3 (51 μM, 20 μg/mL) only increased the mitotic index in the presence of ICRF-193.

(B) Mitotic spreads of cells treated with caffeine and suptopins at the same concentrations as for (A). All cells received an equivalent concentration of DMSO. Nocodazole (332 nM) was added at the time of addition of the suppressors only to ICRF-193 (7 μM) pretreated (6 hr) cells and cells incubated for an additional 12 hr. In the absence of ICRF-193, suptopin-1 and suptopin-2 caused hypercondensed mitotic chromosomes unlike those of DMSO treated cells, whereas mitotic cells treated with caffeine and suptopin-3 appeared normal. In the presence of ICRF-193, caffeine, suptopin-2, and suptopin-3 showed abnormally elongated chromosomes similar to those described in [22]. Suptopin-1-treated cells showed very few to no abnormally elongated chromosomes (none visible in experiment shown).

with fluorescently labeled phalloidin to observe actin microfilaments, a fluorescently labeled anti-α-tubulin antibody to observe the microtubule cytoskeleton, and Hoechst 33342 to observe chromatin (data not shown). None of the compounds appeared to affect the actin cytoskeleton or cause significant alterations in chromatin. However, in interphase cells, suptopin-1 destabilized microtubules, while suptopin-2 and suptopin-3 had no observable effect. In mitotic cells, suptopin-1 caused hypercondensed chromosomes with clearly aberrant spindles, reminiscent of the effects of nocodazole, suptopin-2 caused a disorganized mitotic spindle with an apparent absence of cells in telophase, and suptopin-3 had no observable effect.

Analysis of Cell Cycle and Nuclear Size Using Flow Cytometry

Since suptopin-2 and suptopin-3 had no effect on interphase microtubules, they were chosen for further characterization by dual-parameter flow cytometry, using the TG-3 mAb to measure the number of A549 cells in mitosis, and propidium iodide staining to quantify DNA content (Figures 6A and 6B) [45]. Similar to the mitotic spread analysis, in the absence of ICRF-193, suptopin-2 caused approximately a 6-fold increase in the number of mitotic cells (area III), whereas caffeine and suptopin-3 had no effect. In the presence of ICRF-193 and nocodazole, the number of DMSO-treated mitotic cells (area III) decreased by over half. The number of DMSO-treated cells in G_2 phase, which were negative for TG-3 mAb staining but had a 4 N amount of DNA, increased by over 3-fold. In the presence of ICRF-193 all three compounds—caffeine (15-fold), suptopin-2 (10-fold) and suptopin-3 (6-fold)—caused an increase in the number of TG-3 mAb positive cells with a 4 N amount of DNA, indicating a bypass of the checkpoint arrest.

Besides arresting A549 cells prior to mitosis, an increase in the average diameter of interphase nuclei occurs upon treatment with ICRF-193, a phenotype visible by fluorescent microscopy (data not shown). Correlated with this increase in nuclear size was an increase that was observed during flow cytometry (Figure 6C) in the mean side scatter (SSC), a measure of cellular granularity or complexity, but not forward side scatter (FSC) (data not shown), a measure of cell size. To test whether the increase in SSC was correlated with checkpoint status, SSC measurements were analyzed upon pretreatment of cells with ICRF-193 and a checkpoint suppressor plus nocodazole. While FSC did not change significantly in any of the treatments (data not shown) and none of the chromatid decatenation checkpoint suppressors altered the SSC levels themselves (Figure 6C), the addition of caffeine and, to a lesser extent, suptopin-2 and suptopin-3, decreased SSC in cells pretreated with ICRF-193. These data suggest that the increased granularity of cells upon treatment with ICRF-193 is due to altered chromatin conformation that occurs upon activation of the chromatid decatenation checkpoint.

Effect of Suptopins on Nucleocytoplasmic Transport

Since overexpression of cyclin B1 or treatment of cells with leptomycin B was reported to attenuate the deca-

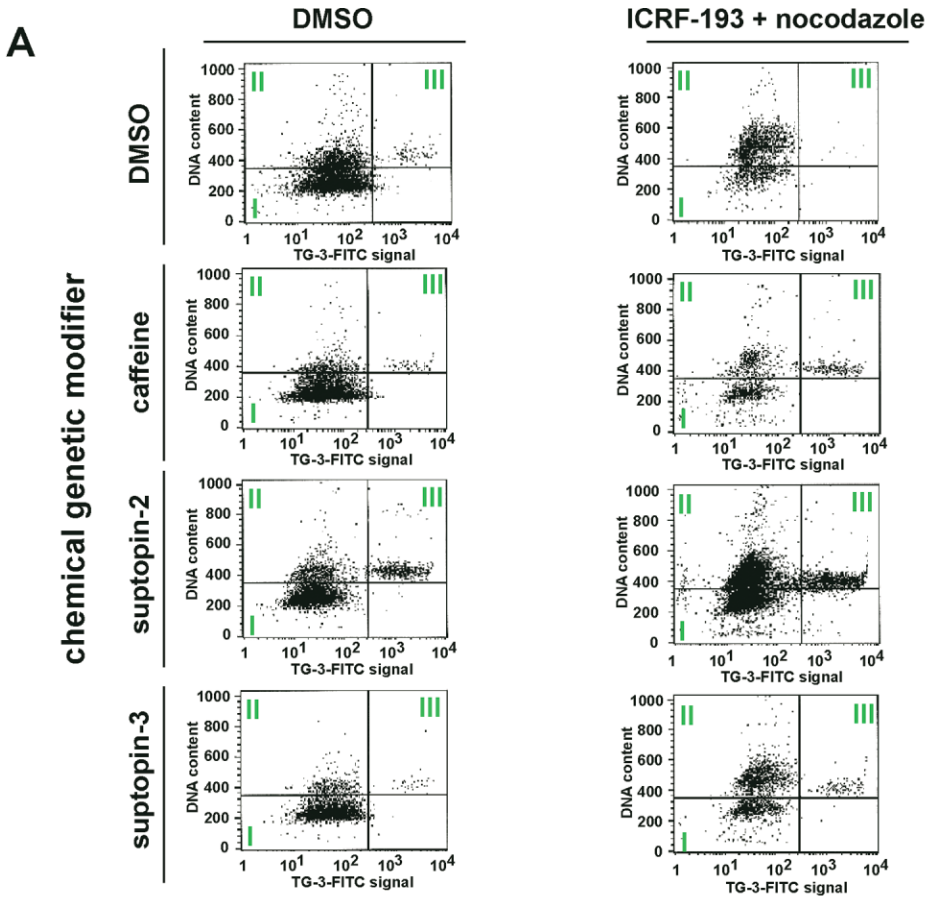

B

DMSO (% of total cells)

area	DMSO	caffeine	suptopin-2	suptopin-3
I	73.6	88.5	67.1	86.4
II	23.1	9.5	18.3	11.7
III	2.3	1.5	14.4	1.3
total cells	81,658	86,677	68,160	47,328

ICRF-193 + nocodazole (% of total cells)

area	DMSO	caffeine	suptopin-2	suptopin-3
I	28.3	52.6	44.8	37.1
II	70	31.7	43.5	56.8
III	0.9	15.3	10.4	5.9
total cells	31,876	25,470	34,623	36,260

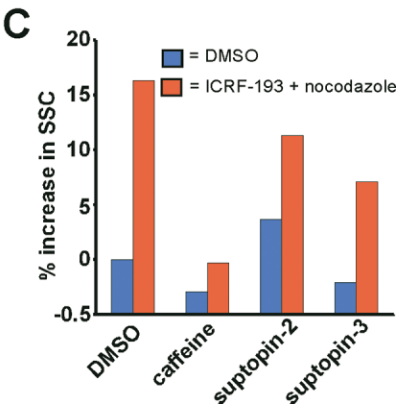

Figure 6. Dual-Parameter Flow Cytometry of the Effect of Suptopin-2 and Suptopin-3 on the Cell Cycle Distribution and Side Scatter (SSC) of A549 Cells

(A) DNA content (y axis) and TG-3-FITC signal (x axis). Suppressors were added for a total of 18 hr. All cells received an equivalent concentration of DMSO. Nocodazole (332 nM) was added at the time of addition of the suppressors only to ICRF-193 (7 μM) pretreated (5 hr) cells. Left panel (DMSO pretreated), suptopin-2 (60 μM, 20 μg/mL), but not caffeine (2 mM) or suptopin-3 (51 μM, 20 μg/mL), increased the mitotic index (area III). Right panel (ICRF-193 pre-treated cells), caffeine (2 mM), suptopin-2 (60 μM, 20 μg/mL), and suptopin-3 (51 μM, 20 μg/mL) all increased the mitotic index (area III).

(B) Quantification of cell cycle distributions in the three areas in (A). Area I, G_1 phase (2 N amount of DNA, low TG-3-FITC signal); Area II, G_2 phase, 4 N amount of DNA, low TG-3-FITC signal); Area III, M phase, 4 N amount of DNA, high TG-3-FITC signal.

(C) Side scatter (SSC), a measure of cellular granularity/complexity, of cells treated with small molecules as in (A). Caffeine and to a lesser extent suptopin-3 and suptopin-2 decreased SSC in the presence of ICRF-193 and nocodazole.

tenation checkpoint [18], we tested whether caffeine or suptopin-1 to -3 affected the cellular localization of cyclin B1 in A549 cells in the presence and absence of ICRF-193. In cells pretreated with DMSO (4 hr), none of these small molecules had a visible effect on the level of expression of cyclin B1 (data not shown). Interestingly,

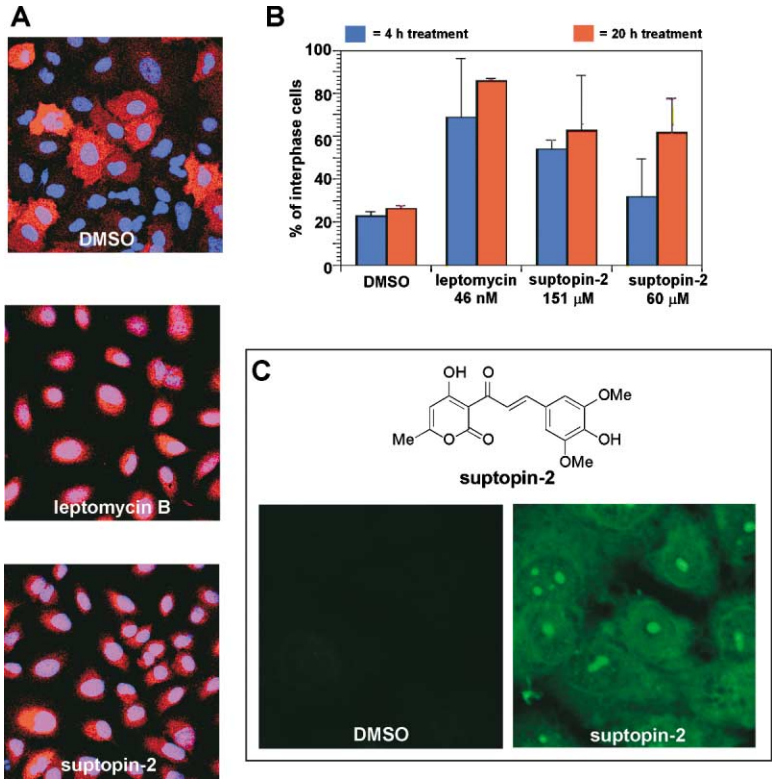

Figure 7. Effect of Suptopin-2 and Leptomycin B on the Intracellular Localization of Cyclin B1 and Fluorescent Properties of Suptopin-2 in A549 Cells

(A) Nuclear (blue, Hoechst 33342) accumulation of cyclin B1 (red; anti-cyclin B1 antibody) in suptopin-2 (120 μM) and leptomycin B (37 nM) treated cells (4 hr) detected using fluorescence microscopy. Nuclei are blue when cyclin B is excluded from the nucleus and pink when it accumulates in the nucleus.

(B) Percentage of cells (average n = 2 treatments, ~100 cells counted per treatment) with cyclin B1 predominantly nuclear detected as in (A). Error bars indicate one standard deviation from the mean.

(C) Intranuclear localization of intrinsic fluorescence (488 nm excitation) from suptopin-2 (151 μM, 20 hr).

suptopin-2 and leptomycin B, but not caffeine, suptopin-1, or suptopin-3, caused the nuclear accumulation of cyclin B1 after a 4 hr treatment (Figure 7A) and increasingly so after a 20 hr treatment (Figure 7B). However, in cells pretreated with ICRF-193 (18 hr), the increased nuclear localization induced by both leptomycin B and suptopin-2 was not observed, perhaps due to altered accumulation of cyclin B1 in the nucleus upon prolonged cell cycle arrest (data not shown). In addition, an accumulation of green fluorescent bi- or single-lobed globular structures within the nucleus of interphase cells was noted upon suptopin-2 treatment (Figure 7C). We speculate that the formation of such structures may sequester nuclear proteins that affect the chromatid decatenation checkpoint. The intrinsic fluorescence of suptopin-2 may prove to be useful in the identification of its target(s) by biochemical means.

The apparent control of cyclin B1 localization by suptopin-2 prompted us to test whether any of the suptopins affect the nucleocytoplasmic transport of other proteins regulated by the Crm1-dependent transporter. To do so, we used as a reporter U2OS cells stably transfected with a human immunodeficiency virus (HIV) Rev-green fluorescent fusion protein (RevGFP) containing a nuclear export sequence recognized by Crm1 [46, 47]. Unlike leptomycin B, which caused nuclear accumulation of the RevGFP reporter [47], suptopin-1 to -3 had little to no effect (Supplemental Figure S2). Although these assays were performed in a different genetic background than the A549 cells and with a reporter protein, this result suggests that suptopin-2 affects the localization of cyclin B1 independent of Crm1-mediated export. Furthermore, the possibility remains that these small molecules affect the nucleocytoplasmic transport of other proteins involved in regulating the chromatid decatenation checkpoint.

Relationship of the Chromatid Decatenation, Chromatin Deacetylation, and Spindle Assembly Checkpoints

One interpretation of the absence of "hit" overlap between the ICRF-193-modifier, TSA-modifier, and antimitotic screens is that the chromatid decatenation, chromatin deacetylation, and spindle assembly checkpoints use different signaling networks in mammalian cells. As a further test for similarities between the signaling networks we determined whether caffeine, an inhibitor of ATR that suppresses the decatenation checkpoint, could suppress the cell cycle effects of trichostatin A. Similarly, we tested again whether ITSA1, a suppressor of trichostatin A, could suppress the cell cycle effects of ICRF-193. These experiments showed that caffeine has no effect on the cell cycle arrest or on the level of histone H3 acetylation and α-tubulin acetylation (data not shown) induced by trichostatin A and that ITSA1 had no effect on the cell cycle arrest induced by ICRF-193 (Supplemental Figure S3). Collectively, these results support the notion that the chromatid decatenation checkpoint functions independently from the chromatin deacetylation checkpoint.

Discussion

The small molecule library used in this study is a commercially available collection of compounds possessing a diverse range of structural properties and chemical

functionalities. For example, the values (low, high, average, median) for molecular weights (g/mol) are 157.21, 698.9, 337.73, 322.36, respectively; for calculated solubility (cLogP) are −4.69, 9.76, 2.97, 2.99, respectively; for the number of hydrogen bond donors are 0, 10, 1.33, 1, respectively; and for the number of hydrogen bond acceptors are 0, 24, 5.69, 5, respectively (see http://iccb.med.harvard.edu/screening/compound_libraries/chembridge_additional.html for more details). However, without rigorous comparison to a collection of reference molecules or some other standard, it is difficult to draw precise conclusions about the chemical diversity of the library. Regardless, the dispersion of the four classes of biological activity across the global map of the chemical space derived from principal component analysis of the associated molecular descriptors indicates that no particular region of chemical space was favored by any one of the three assays. These results demonstrate that small molecules with very different structures can have the same phenotypic effect in cell-based assays. This property may derive from the small molecules each targeting different nodes in the networks regulating the particular cellular processes involved. Alternatively, as exemplified by the small molecules targeting tubulin [41], a diverse range of structures may be capable of affecting a particular protein. In either case, these results highlight the challenging nature of structure-based prediction of biological activity and the derivation of structure-activity models using cell-based screening data only.

Although the mechanism(s) of action of the suptopins remain unknown, our findings point to the role of suptopin-2 in regulating nucleocytoplasmic transport. As has been observed for the DNA damage-induced G_2 checkpoint, the regulation of the location and activity of Cdk1 and its regulatory subunit cyclin B are key aspects of the cellular response to altered genomic stability [29]. Cyclin B1's localization is regulated by Crm1, a member of a karyopherin family of nucleocytoplasmic transport receptors [27]. Although suptopin-2 does not appear to be a general inhibitor of Crm1-mediated transport based upon the Rev-GFP assay (Supplemental Figure S2), it may specifically interact with a component unique to cyclin B transport or through a mechanism independent of Crm1. We note that in contrast to the results described in [18], we did not observe a leptomycin B-induced increase in the number of condensed mitotic chromosomes in the presence of ICRF-193 (data not shown). These differences may be due to the different genetic backgrounds of the cell lines used, duration of treatment, or concentration of leptomycin B.

Since variation exists in the relative affinities of different small molecule-protein interactions, the stability of different organic molecules, and the abundance of cellular proteins, some small molecules may have multiple and sometimes competing effects in cells at different concentrations. Such pleiotropy would explain the ability of suptopin-1 and suptopin-2 to increase the mitotic index in the absence of ICRF-193. Alternatively, since 13-hydroxy-15-oxozoapatlin, a recently identified suppressor of the DNA-damage induced G_2 checkpoint, also causes mitotic spindle defects [39], such effects might be a common property of suppressors of the G_2 checkpoints that act different mechanistically from caffeine. Of the compounds analyzed here, suptopin-3 was the most like caffeine in terms of its ability to bypass the decatenation checkpoint without having an effect on microtubule stability or causing nuclear accumulation of cyclin B1. Thus, we hypothesize that the cellular interactions of suptopin-3 are more specifically related to the chromatid decatentation checkpoint than those of suptopin-1 or suptopin-2.

Unlike the DNA damage G_2 checkpoint [1, 2], the induction of the chromatid decatenation checkpoint with ICRF-193 has been reported to be independent of ATM signaling and to occur in the absence of Chk1 and Chk2 phosphorylation [18, 20]. However, it is important to note that although there is evolutionary conservation of the chromatid decatenation checkpoint across at least two metazoan kingdoms (plants and animals) [2], its existence, at least to date, depends entirely on the use of bis(2,6-dioxopiperazine) derivatives. Thus, if ICRF-193 or the closed-clamp form of TopoII have additional effects on cells, then the induction of the G(2) phase could be due to these other activities [20]. Some support for this possibility exists [48–50]; thus, it is possible that the suptopins suppress the cell cycle arrest induced by ICRF-193 through an effect on pathways related to these other activities of ICRF-193.

An emerging application of checkpoint suppressors is for the sensitization of tumor cells to damage arising as a result of altering DNA metabolism (reviewed in [51]). While cancer treatment often involves combination therapy of multiple chemotherapeutics agents, the notion of sensitizing cells to the effects of a chemotherapeutic agent by simultaneously eliminating the cellular response that leads to the perturbations has only recently begun to be explored systematically. One notable exception from a theoretical perspective was the use of caffeine by Pardee [52], which can now be rationalized due to the inhibition of ATR [24–26]. If eliminating the chromatid decatenation checkpoint sensitizes tumor cells to genomic instability, then one attractive feature of suppressors like the suptopins is that they may operate without affecting DNA damage checkpoints. This might reduce the likelihood that treatment with such a checkpoint suppressor leads to mutations in otherwise normal cells.

In summary, the analysis of multidimensional datasets using methods of dimensionality reduction and unsupervised clustering, such as hierarchical clustering and principal component analysis (for example, Figures 3 and 4), provide a biologically based means of analyzing the diversity of small molecules and their effects on biological systems. These global methods of analysis may become increasingly powerful discovery tools in the context of rapidly growing numbers of diverse small molecule modulators and other methods of chemical perturbation, such as ribonucleic acid interference (reviewed in [53]). By combining the results of multiple cell-based assays, phenotypic effects of small molecules can be mapped onto a multidimensional space derived from molecular descriptors analysis yielding a "functional map" of chemical space (Figure 3D).

Significance

Although there is growing interest in the use of small molecules as basic research tools, there remains a

relative paucity of such molecules and only limited approaches to enable their discovery. The chemical genetic modifier screen used here to identify small molecule modulators of the human chromatid decatenation checkpoint illustrates an approach that should be applicable to the dissection of signaling networks involved in the regulation of other aspects of cell proliferation, as well as the mechanism of action, development of resistance to, and metabolism of chemotherapeutics. Using this approach in the current study, we provide evidence that the chromatid decatenation functions independently from the chromatin deacetylation checkpoint. Through consideration of multiple screening datasets, these results provide an example of mapping chemical space using a combination of phenotypic and molecular descriptors. The suptopins provide new molecular tools for investigating the molecular mechanism regulating genomic stability in general and, more specifically, for illuminating whether inhibiting the chromatid decatenation checkpoint sensitizes tumor cells to certain chemotherapeutic agents.

Experimental Procedures

Materials

Trichostatin A, nocodazole, and ribonuclease A were purchased from Sigma. Propidium iodide, Hoechst 33342, Hoechst 33258, and Texas methyl red-conjugated anti-mouse IgG antibody were purchased from Molecular Probes. ITSA1 (5253409), suptopin-1 (5146479), suptopin-2 (5118575), and suptopin-3 (5244640) were purchased from ChemBridge. ICRF-193 was a gift from Dr. James Wang (Harvard University). Fluorescein isothiocyanate-conjugated anti-mouse IgM was purchased from Calbiochem. Enhanced chemiluminescent reagents were purchased from Amersham Pharmacia. Anti-cyclin B1 antibody was purchased from Santa Cruz. Anti-TG-3 mAb was a gift from Dr. Peter Davies (Albert Einstein College of Medicine). 384-well pin arrays were purchased from Genetix. X-OMAT AR film was purchased from Kodak Corporation. FuGENE 6 transfection regents were purchased from Boehinger Mannheim. All cell culture reagents were purchased from Gibco, BRL.

Cell Culture

A549 cells (ATCC, human lung carcinoma) were maintained at 37°C, 5% CO_2 in Dulbecco's modified Eagle medium (DMEM) supplemented with 10% fetal bovine serum (FBS), 100 units/mL penicillin G sodium, 100 μg/ml streptomycin sulfate (1% P/S), and 2 mM L-glutamine (1% L-Gln) ($DMEM^+$). U2OS (human osteosarcoma)-RevGFP cells were maintained as for A549 cells and grown in DMEM containing 10% Fetal Clone ($DMEM^C$). These cells were established by transfecting U2OS cells with pRev(1.4)-GFP+PKI NES (gift from Dr. Beric Henderson [47]) with FuGENE 6 according to the manufacturer's directions. Stable clones were selected in complete media containing 400 μg/mL G418.

TG-3 Cytoblot Assay

A549 cells were seeded in 45 μl $DMEM^+$ (4000 cells/well) in white 384-well plates (Nalge Nunc, tissue culture treated) using a liquid dispenser (Multidrop 384, Labsystems) and allowed to attach overnight at 37°C with 5% CO_2. ICRF-193 (5 μl) ([final] = 7 μM) was added to each well, and incubation continued for 5 hr. Since ICRF-193 is dominant to the addition of nocodazole, cells are prevented from entering mitosis and the basal signal from the mitosis-specific phosphorylation-sensitive epitope recognized by the TG-3 mAb was low [36]. Library compounds (9600 molecules, Diverse E set, ChemBridge) dissolved in DMSO (5 mg/ml) were then pin transferred (50–200 nL to each well, [final] = ~20 μM/well) using disposable 384-well pin arrays and nocodazole (332 nM final concentration), a microtubule destabilizer, added to arrest cells that have bypassed the checkpoint and entered mitosis. Following 16 hr incubation, the number of cells in mitosis was assayed using the TG-3 mAb as described in [40] using a horseradish peroxidase-conjugated anti-mouse IgM antibody and enhanced chemiluminescent reagents. Data was collected on an Analyst plate reader (LJL Biosystems) with an integration time of 0.1 s. For film detection of cytoblots, film was placed on top of the plate for 1–5 min and then developed in a Kodak M35A X-OMAT processor. After two rounds of retesting, small molecules that had a TG-3 mAb signal equal to (or greater than) the mean plus 1.5 standard deviations of DMSO-treated control cells were considered to be biologically active.

Multidimensional Assay and Molecular Descriptor Analysis

Hierarchical clustering of binary (0 = no hit, 1 = hit) screening results was performed using the unweighted pair-group average method with the Tanimoto distance metric (XLStat-Pro v5.2). A structure descriptor file containing each small molecule was imported into QSARIS (SciVision, Inc.) for enumeration of a set of 221 graph and information theoretic and physiochemical descriptors. 3-D descriptors were computed using an energy-minimized conformation. Descriptors with zero variance were removed before importing data into Microsoft Excel and performing principal component analysis (XLStat-Pro v5.2). In the calculation of the global chemical space, small molecules with missing values (for example due to the presence of a counter ion) were removed from the analysis leaving a total of 15,120 small molecules. In the calculation of the local chemical space of only the ICRF-193 suppressors, missing values for two small molecules (51 N16 and 37 A17) were replaced by the descriptor means. Visualization of 3-dimensional PCA models was performed by importing the coordinates of compounds after PCA into Spotfire Descision Site software (v7.0).

Fluorescence Microscopy

For mitotic spreads, A549 cells (~75% confluent) in 10 cm dishes treated as indicated were trypsinized cells and pelleted (2 min) at 1000 rpm on a Beckman tabletop centrifuge. The supernatant was aspirated and 1 ml of 75 mM potassium chloride added to swell cells (10 min). Cells were pelleted, supernatant aspirated, and cells resuspendend in 0.5 ml Carnoy's fixative (1:3 acetic acid:methanol, −20°C, 10 min). Cells were pelleted and all but 50–100 μl of the supernatant aspirated. After resuspending, ~15 μl per sample was spotted from a height of 10 cm onto glass slides and allowed to dry before staining (10 min) with Hoechst (1 μg/mL in Tris-buffered saline [TBS] and mounting. For detection of microtubules and actin (data not shown), A549 cells were seeded onto glass coverslips at 80%–90% confluency, and small molecules added after diluting in cellular medium. Cells were fixed in glutaraldehyde (0.2%) in a permeabilization buffer (50 mM K-Pipes [pH 6.8], 5 mM EGTA, 0.5 mM $MgCl_2$, and 0.1% Triton X-100) for 15 min, quenched (10 min) in sodium borohydride (10 mg/mL) in TBS/0.1% Triton X-100 (TBS-T), and stained with fluorescein isothiocyanate-conjugated (FITC)-conjugated anti-α-tubulin antibody (DM1α; 1:500), TMR-conjugated phalloidin (2 μg/mL), and Hoechst 33342 (1 μg/mL) diluted in antibody dilution buffer (ADB, TBS-T/2% bovine serum albumin/0.1% sodium azide). For detection of cyclin B1, cells were fixed in methanol (100%, −20°C, 5–20 min), washed twice in ADB and blocked overnight in ADB. Cells were stained with an anti-cyclin B1 antibody (1:50) and Hoechst 33342 (1 μg/ml) dye diluted ADB followed by a secondary TMR-conjugated anti-mouse IgG antibody (1:500). For detection of suptopin-2 fluorescence, A549 cells were illuminated between 364 and 514 nm using a longpass filter, with a peak emission occurring at an excitation wavelength of 488 nm, and no emission occurring at or above 543 nm. Images of mitotic spreads were collected on a Leitz Laborlux 2 microscope with a 40× PHACO2 objective. Images of microtubule/actin cytoskeleton (data not shown) and cyclin B1 localization were collected on a Zeiss LSM510 confocal scanning laser microscope using a 63× objective using the accompanying software. For the RevGFP export assay, U2OS-RevGFP cells were seeded onto clear-bottom, black 384-well plates (Costar) at a density of ~4500 cells/well in 50 μl $DMEM^C$. Cells were allowed to attach and grow overnight before compound treatment. Compounds were diluted 1:125 in DMEM and serially diluted 1:2 in a separate 384-well plate. Media was aspirated from cells before the diluted compounds were transferred onto them. Cells were incubated with compound for ~1 hr before fixation with 3.7% formalde-

hyde and nuclei staining with Hoechst 33258 at 2 μg/mL. RevGFP localization was then imaged with an inverted fluorescence microscope containing a 20× ELWD objective (Nikon) and Metamorph software (Universal Imaging).

Flow Cytometry

A549 cells (~75% confluent) in 10 cm dishes were pretreated with DMSO (0.1% v/v) or ICRF-193 (7 μM) for 6 hr. Small molecules were added at the indicated concentrations for an additional 18 hr. Samples were rinsed in PBS, trypsinized, fixed (30 min, 3.7% formaldehyde in TBS, room temperature; 5 min 100% methanol [−20°C], washed in TBS/1% bovine serum albumin (TBS-B), and stored overnight in TBS-B (4°C). To determine the number of cells in M phase [45], samples were washed and incubated (4°C; shaking) in ADB with TG-3 mAb (1:60 v/v from ascites fluid) and FITC-conjugated anti-mouse IgM (1:200 v/v, for 9 hr). Cells were washed three times (2 mL) of TBS, resuspended in ribonuclease A (100 μL, 100 μg/mL), and incubated 10 min (37°C). To measure the DNA content, propidium iodide ([PI] 400 μL, 50 μg/mL) was added and incubated 1 hr at room temperature. Samples were analyzed using a FACScanII flow cytometer (Becton-Dickinson) at the Dana Farber Cancer Institute, exciting at 488 nm and measuring PI fluorescence through a 600 nm band-pass filter. Cell cycle distributions and apoptosis analysis were modeled using ModFit LT (v2.0) software. Side scatter (SSC) measurements, which are affected by the granularity or complexity of cellular contents upon laser excitation, were collected while sorting cells.

Acknowledgments

We are grateful to Dr. James Wang for the gift of ICRF-193, Dr. Paul Clemons for the generation of the molecular descriptors, as well as other members of the Schreiber group for helpful discussions. S.L.S. is an Investigator at the Howard Hughes Medical Institute in the Department of Chemistry & Chemical Biology, Harvard University. We thank the National Institute for General Medical Sciences for support of this research (GM38627); the National Cancer Institute (NCI), Merck KGaA, Merck & Co., and the Keck Foundation for support of ICCB; and the NCI for support of the Initiative for Chemical Genetics. K.M.K. was supported by a Damon Runyon Cancer Research Foundation Fellowship (DRG-1650).

Received: August 15, 2003
Revised: October 1, 2003
Accepted: October 14, 2003
Published: December 19, 2003

References

1. Nyberg, K.A., Michelson, R.J., Putnam, C.W., and Weinert, T.A. (2002). Toward maintaining the genome: DNA Damage and Replication Checkpoints. Annu. Rev. Genet. *36*, 617–656.
2. Smith, A.P., Gimenez-Abian, J.F., and Clarke, D.J. (2002). DNA-damage-independent checkpoints: yeast and higher eukaryotes. Cell Cycle *1*, 16–33.
3. Swedlow, J.R., and Hirano, T. (2003). The making of the mitotic chromosome. Modern insights into classical questions. Mol. Cell *11*, 557–569.
4. Nasmyth, K. (2002). Segregating sister genomes: the molecular biology of chromosome separation. Science *297*, 559–565.
5. Holloway, S.L. (1995). Sister chromatid separation in vivo and in vitro. Curr. Opin. Genet. Dev. *5*, 243–248.
6. Holm, C. (1994). Coming undone: how to untangle a chromosome. Cell *77*, 955–957.
7. Wang, J.C. (2002). Cellular roles of DNA topoisomerases: a molecular perspective. Nat. Rev. Mol. Cell Biol. *3*, 430–440.
8. Kaufmann, W.K. (1998). Human topoisomerase II function, tyrosine phosphorylation and cell cycle checkpoints. Proc. Soc. Exp. Biol. Med. *217*, 327–334.
9. Wilstermann, A.M., and Osheroff, N. (2003). Stabilization of eukaryotic topoisomerase II-DNA cleavage complexes. Curr. Top. Med. Chem. *3*, 321–338.
10. Andoh, T., and Ishida, R. (1998). Catalytic inhibitors of DNA topoisomerase II. Biochim. Biophys. Acta *1400*, 155–171.
11. Abraham, R.T. (2001). Cell cycle checkpoint signaling through the ATM and ATR kinases. Genes Dev. *15*, 2177–2196.
12. Shiloh, Y. (2001). ATM and ATR: networking cellular responses to DNA damage. Curr. Opin. Genet. Dev. *11*, 71–77.
13. Wang, Y., Cortez, D., Yazdi, P., Neff, N., Elledge, S.J., and Qin, J. (2000). BASC, a super complex of BRCA1-associated proteins involved in the recognition and repair of aberrant DNA structures. Genes Dev. *14*, 927–939.
14. Futaki, M., and Liu, J.M. (2001). Chromosomal breakage syndromes and the BRCA1 genome surveillance complex. Trends Mol. Med. *7*, 560–565.
15. Tanabe, K., Ikegami, Y., Ishida, R., and Andoh, T. (1991). Inhibition of topoisomerase II by antitumor agents bis(2,6-dioxopiperazine) derivatives. Cancer Res. *51*, 4903–4908.
16. Downes, C.S., Clarke, D.J., Mullinger, A.M., Gimenez-Abian, J.F., Creighton, A.M., and Johnson, R.T. (1994). A topoisomerase II-dependent G2 cycle checkpoint in mammalian cells. Nature *372*, 467–470.
17. Kaufmann, W.K., and Kies, P.E. (1998). DNA signals for G2 checkpoint response in diploid human fibroblasts. Mutat. Res. *400*, 153–167.
18. Deming, P.B., Cistulli, C.A., Zhao, H., Graves, P.R., Piwnica-Worms, H., Paules, R.S., Downes, C.S., and Kaufmann, W.K. (2001). The human decatenation checkpoint. Proc. Natl. Acad. Sci. USA *98*, 12044–12049.
19. Munoz, P., Baus, F., and Piette, J. (2001). Ku antigen is required to relieve G2 arrest caused by inhibition of DNA topoisomerase II activity by the bisdioxopiperazine ICRF-193. Oncogene *20*, 1990–1999.
20. Deming, P.B., Flores, K.G., Downes, C.S., Paules, R.S., and Kaufmann, W.K. (2002). ATR enforces the topoisomerase II-dependent G2 checkpoint through inhibition of Plk1 kinase. J. Biol. Chem. *277*, 36832–36838.
21. Kaufmann, W.K., Campbell, C.B., Simpson, D.A., Deming, P.B., Filatov, L., Galloway, D.A., Zhao, X.J., Creighton, A.M., and Downes, C.S. (2002). Degradation of ATM-independent decatenation checkpoint function in human cells is secondary to inactivation of p53 and correlated with chromosomal destabilization. Cell Cycle *1*, 210–229.
22. Andreassen, P.R., Lacroix, F.B., and Margolis, R.L. (1997). Chromosomes with two intact axial cores are induced by G2 checkpoint override: evidence that DNA decatenation is not required to template the chromosome structure. J. Cell Biol. *136*, 29–43.
23. Anderson, H., and Roberge, M. (1996). Topoisomerase II inhibitors affect entry into mitosis and chromosome condensation in BHK cells. Cell Growth Differ. *7*, 83–90.
24. Jiang, X., Lim, L.Y., Daly, J.W., Li, A.H., Jacobson, K.A., and Roberge, M. (2000). Structure-activity relationships for G2 checkpoint inhibition by caffeine analogs. Int. J. Oncol. *16*, 971–978.
25. Sarkaria, J.N., Busby, E.C., Tibbetts, R.S., Roos, P., Taya, Y., Karnitz, L.M., and Abraham, R.T. (1999). Inhibition of ATM and ATR kinase activities by the radiosensitizing agent, caffeine. Cancer Res. *59*, 375–382.
26. Nghiem, P., Park, P.K., Kim, Y., Vaziri, C., and Schreiber, S.L. (2001). ATR inhibition selectively sensitizes G1 checkpoint-deficient cells to lethal premature chromatin condensation. Proc. Natl. Acad. Sci. USA *98*, 9092–9097.
27. Kudo, N., Matsumori, N., Taoka, H., Fujiwara, D., Schreiner, E.P., Wolff, B., Yoshida, M., and Horinouchi, S. (1999). Leptomycin B inactivates CRM1/exportin 1 by covalent modification at a cysteine residue in the central conserved region. Proc. Natl. Acad. Sci. USA *96*, 9112–9117.
28. Hagting, A., Karlsson, C., Clute, P., Jackman, M., and Pines, J. (1998). MPF localization is controlled by nuclear export. EMBO J. *17*, 4127–4138.
29. Toyoshima, F., Moriguchi, T., Wada, A., Fukuda, M., and Nishida, E. (1998). Nuclear export of cyclin B1 and its possible role in the DNA damage-induced G2 checkpoint. EMBO J. *17*, 2728–2735.
30. Johnstone, R.W., and Licht, J.D. (2003). Histone deacetylase inhibitors in cancer therapy: is transcription the primary target? Cancer Cell *4*, 13–18.

31. Qiu, L., Burgess, A., Fairlie, D.P., Leonard, H., Parsons, P.G., and Gabrielli, B.G. (2000). Histone deacetylase inhibitors trigger a G2 checkpoint in normal cells that is defective in tumor cells. Mol. Biol. Cell *11*, 2069–2083.
32. Yoshida, M., Kikima, M., Akita, M., and Beppu, T. (1990). Potent and specific inhibition of mammalian histone deacetylase both in vivo and in vitro by trichostatin A. J. Biol. Chem. *265*, 17174–17179.
33. Koeller, K.M., Haggarty, S.J., Perkins, B.D., Leykin, I., Wong, J.C., Kao, M.C., and Schreiber, S.L. (2003). Chemical genetic modifier screens. Small molecule trichostatin suppressors as probes of intracellular histone and tubulin acetylation. Chem. Biol. *10*, 397–410.
34. Tsai, S.C., Valkov, N., Yang, W.M., Gump, J., Sullivan, D., and Seto, E. (2000). Histone deacetylase interacts directly with DNA topoisomerase II. Nat. Genet. *26*, 349–353.
35. Johnson, C.A., Padget, K., Austin, C.A., and Turner, B.M. (2001). Deacetylase activity associates with topoisomerase II and is necessary for etoposide-induced apoptosis. J. Biol. Chem. *276*, 4539–4542.
36. Jicha, G.A., Lane, E., Vincent, I., Otvos, L., Jr., Hoffmann, R., and Davies, P. (1997). A conformation- and phosphorylation-dependent antibody recognizing the paired helical filaments of Alzheimer's disease. J. Neurochem. *69*, 2087–2095.
37. Roberge, M., Berlinck, R.G., Xu, L., Anderson, H.J., Lim, L.Y., Curman, D., Stringer, C.M., Friend, S.H., Davies, P., Vincent, I., et al. (1998). High-throughput assay for G2 checkpoint inhibitors and identification of the structurally novel compound isogranulatimide. Cancer Res. *58*, 5701–5706.
38. Curman, D., Cinel, B., Williams, D.E., Rundle, N., Block, W.D., Goodarzi, A.A., Hutchins, J.R., Clarke, P.R., Zhou, B.B., Lees-Miller, S.P., et al. (2001). Inhibition of the G2 DNA damage checkpoint and of protein kinases Chk1 and Chk2 by the marine sponge alkaloid debromohymenialdisine. J. Biol. Chem. *276*, 17914–17919.
39. Rundle, N.T., Xu, L., Andersen, R.J., and Roberge, M. (2001). G2 DNA damage checkpoint inhibition and antimitotic activity of 13-hydroxy-15-oxozoapatlin. J. Biol. Chem. *276*, 48231–48236.
40. Stockwell, B.R., Haggarty, S.J., and Schreiber, S.L. (1999). High-throughput screening of small molecules in miniaturized mammalian cell-based assays involving post-translational modifications. Chem. Biol. *6*, 71–83.
41. Haggarty, S.J., Mayer, T.U., Miyamoto, D.T., Fathi, R., King, R.W., Mitchison, T.J., and Schreiber, S.L. (2000). Dissecting cellular processes using small molecules: identification of colchicine-like, taxol-like and other small molecules that perturb mitosis. Chem. Biol. *7*, 275–286.
42. Mayer, T.U., Kapoor, T.M., Haggarty, S.J., King, R.W., Schreiber, S.L., and Mitchison, T.J. (1999). Small molecule inhibitor of mitotic spindle bipolarity identified in a phenotype-based screen. Science *286*, 971–974.
43. Hotelling, H. (1931). Analysis of a complex of statistical variables into principal components. J. Educ. Psychol. *24*, 417–441.
44. Legendre, P., and Legendre, L. (1998). Numerical Ecology—Developments in Environmental Modeling (New York: Elsevier).
45. Anderson, H.J., de Jong, G., Vincent, I., and Roberge, M. (1998). Flow cytometry of mitotic cells. Exp. Cell Res. *238*, 498–502.
46. Kau, T.R., and Silver, P.A. (2003). Nuclear transport as a target for cell growth. Drug Discov. Today *8*, 78–85.
47. Henderson, B.R., and Eleftheriou, A.A. (2000). Comparison of the activity, sequence specificity, and CRM1-dependence of different nuclear export signals. Exp. Cell Res. *10*, 213–224.
48. Jensen, L.H., Nitiss, K.C., Rose, A., Dong, J., Zhou, J., Hu, T., Osheroff, N., Jensen, P.B., Sehested, M., and Nitiss, J.L. (2000). A novel mechanism of cell killing by anti-topoisomerase II bisdioxopiperazines. J. Biol. Chem. *275*, 2137–2146.
49. Xiao, H., Mao, Y., Desai, S.D., Zhou, N., Ting, C.Y., Hwang, J., and Liu, L.F. (2003). The topoisomerase IIbeta circular clamp arrests transcription and signals a 26S proteasome pathway. Proc. Natl. Acad. Sci. USA *100*, 3239–3244.
50. Huang, K.C., Gao, H., Yamasaki, E.F., Grabowski, D.R., Liu, S., Shen, L.L., Chan, K.K., Ganapathi, R., and Snapka, R.M. (2001). Topoisomerase II poisoning by ICRF-193. J. Biol. Chem. *276*, 44488–44494.
51. Tenzer, A., and Pruschy, M. (2003). Potentiation of DNA-damage-induced cytotoxity by G(2) checkpoint abrogators. Curr. Med. Chem. Anti-Canc. Agents *3*, 35–46.
52. Fingert, H.J., Chang, J.D., and Pardee, A.B. (1986). Cytotoxic, cell cycle, and chromosomal effects of methylxanthines in human tumor cells treated with alkylating agents. Cancer Res. *46*, 2463–2467.
53. McManus, M.T., and Sharp, P.A. (2002). Gene silencing in mammals by small interfering RNAs. Nat. Rev. Genet. *3*, 737–747.